

A New Gastric Histopathology Subsize Image Database (GasHisSDB) for Classification Algorithm Test: from Linear Regression to Visual Transformer

Weiming Hu^a, Chen Li^{a,*}, Xiaoyan Li^b, Haoyuan Chen^a, Wanli Liu^a, Changhao Sun^a and Marcin Grzegorzec^c

^aMicroscopic Image and Medical Image Analysis Group, MBIE College, Northeastern University, 110169, Shenyang, PR China

^bDepartment of Pathology, Cancer Hospital, China Medical University, Liaoning Cancer Hospital and Institute, Shenyang 110042, PR China

^cInstitute of Medical Informatics, University of Luebeck, Luebeck, Germany

ARTICLE INFO

Keywords:

Gastric Histopathology
Subsize Image
Database
Image classification

ABSTRACT

GasHisSDB is a New Gastric Histopathology Subsize Image Database with a total of 245196 images. GasHisSDB is divided into 160×160 pixels sub-database, 120×120 pixels sub-database and 80×80 pixels sub-database. GasHisSDB is made to realize the function of evaluating image classification. In order to prove that the methods of different periods in the field of image classification have discrepancies on GasHisSDB, we select a variety of classifiers for evaluation. Seven classical machine learning classifiers, three CNN classifiers and a novel transformer-based classifier are selected for testing on image classification tasks. GasHisSDB is available at the URL: <https://github.com/NEUhwmm/GasHisSDB.git>.

1. Introduction

Gastric cancer is a common type of malignant tumor with relatively poor prognosis and presents a serious threat to global health [1]. According to the recent Global Cancer Statistics, gastric cancer is the fifth commonly diagnosed cancer [2], and deaths from gastric cancer is 18.0% of the total cancer deaths [2]. Histopathological examination of gastric cancer is a microscopic examination of paraffin sections made from tissues taken from suspected cancer sites by experienced pathologists, and histology should be reported according to the World Health Organisation criteria [3]. This is the gold-standard for gastric cancer diagnosis and a basic requirement prior to treatment initiation [1].

Hematoxylin and Eosin (H & E) staining is one of the commonly used staining methods in paraffin section technology used for demonstration of nucleus and cytoplasmic inclusions in clinical specimens, and it is capable of highlighting the fine structures of cells and tissues [4, 5, 6]. Firstly, the pathological section is observed with naked eye to observe whether the section is qualified or not and to roughly find the lesion, when H & E staining pathological section of gastric cancer is diagnosed. Then the main step is to use low magnification microscope to observe and diagnose. If doctors want to observe the fine structure of the lesion more clearly, they can move it to the center of the vision fields, switch to high-power microscopy and make diagnosis [7]. It can be seen that there are the following problems in the process of observing H & E staining sections of gastric cancer: the diagnosis results of medical doctors are subjective and hard to be quantitative described, their workload is heavy, and working hours are long, it is easy for doctors to omit section in-

formation, and it is inconvenient to use big data technology. Therefore, there is an urgent need for more efficient solutions to related problems.

Nowadays, with the rapid development of computer vision technology, especially the emergence of medical image classification, these technologies can objectively examine every electron microscope photo of gastric cancer pathological section, and process a large number of data quickly and efficiently. Thus, it brings an opportunity to solve the above problems in the diagnosis of gastric cancer [8, 9, 10]. Especially, image classification plays an important role in computer-aided diagnosis. In the field of distinguishing benign or malignant tumors, distinguishing the differentiation stage of tumors and distinguishing the subtype of cancer, the results of image classification methods can be used as an important reference for clinicians to make diagnosis. Furthermore, with the development of medical image classification technology, the main purpose of this technology is not only to achieve high accuracy, but also to have high anti-interference ability [11, 12]. Although the mainstream trend is to scan the whole-slide images for analysis, the actual work often encounter the actual situation of computer performance shortage, where the whole-slide images are usually cropped into many subsize images for analysis. To this end, we need a Subsize Image Database to test the anti-interference ability of various medical image classification technologies [13].

In this paper, we introduce a novel public available *Gastric Histopathology Subsize Image Database* (GasHisSDB), which consists of 245196 subsize pathological images of gastric cancer and contains three subsize levels. Each level of the database includes two categories (normal tissue region images and cancerous tissue images). Furthermore, each image in this database calculates five different features, charac-

*Corresponding author

✉ lichen201096@hotmail.com (C. Li)

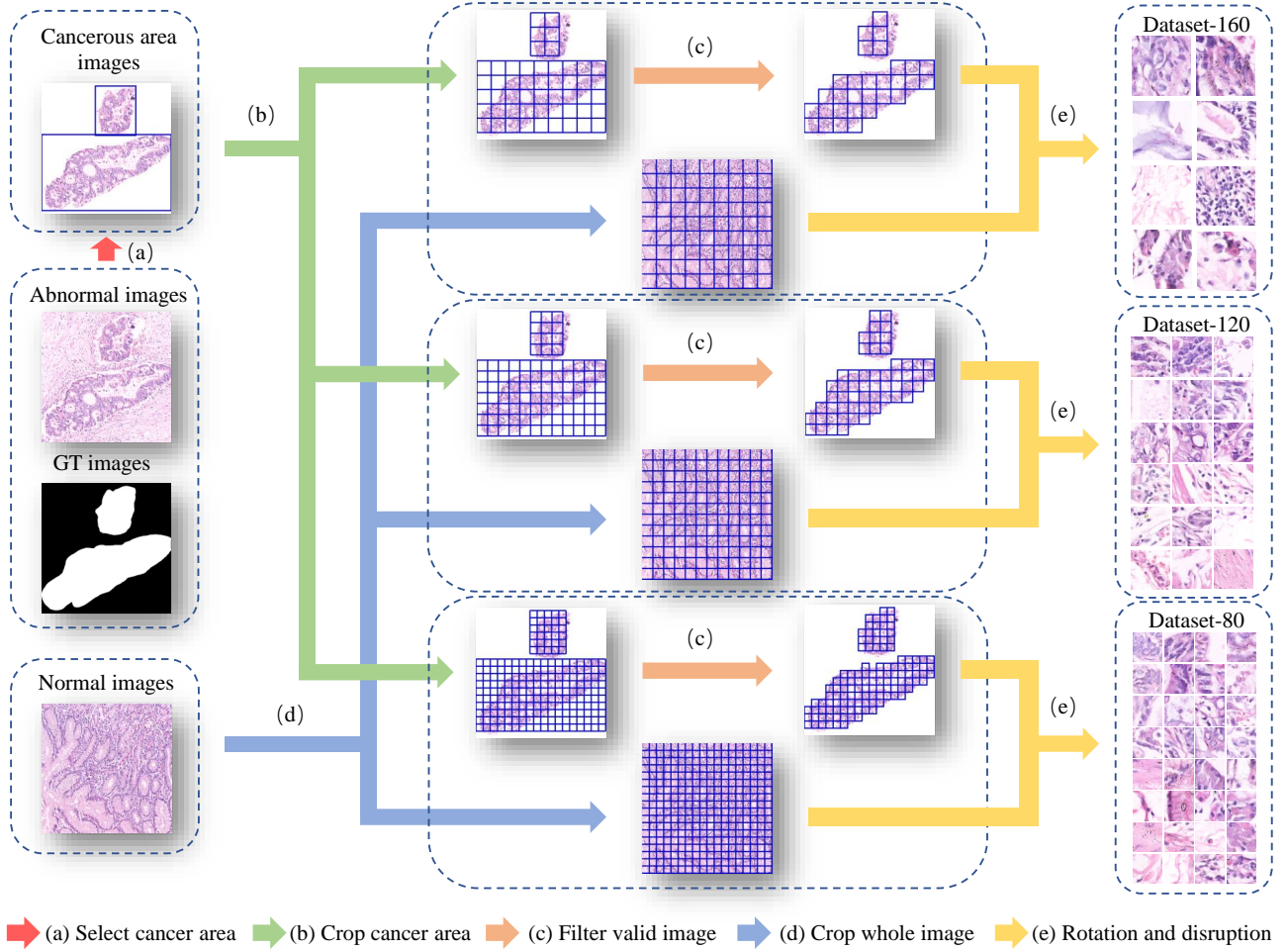


Figure 1: Data preparation workflow of GasHisSDB.

terizing the color, the intensity and the texture. Finally, we give the evaluation results of classification schemes based on features and images, use machine learning method and new deep learning method, and evaluate the discrimination ability of each classifier.

2. GasHisSDB

2.1. Database preparation

The preparation process of this database is as follows: firstly, three sizes (160×160 , 120×120 , 80×80 pixels) of normal pathological sections are cropped directly. However, when dealing with abnormal pathological sections, it is necessary to select the cancerous region as the region of interest. The region of interest of pathological section is cropped, and the ground truth is cropped simultaneously. This work can be used to filter out images with too few cancerous areas. Furthermore, in order to reduce the correlation among subsize images from the same original images, each one is rotated randomly and the image order of the whole database is scrambled. The data preparation workflow of GasHisSDB

is shown in Figure. 1.

2.2. Database overview

GasHisSDB contains 245196 subsize images. These images are programmatically cropped by the pathological images of gastric cancer with H & E staining obtained by optic microscope from a basic public dataset [14, 15]. The dataset scale is represented in Table. 1.

Table 1
Dataset scale of GasHisSDB.

Cropping size	Abnormal	Normal
160×160 pixels	13,124	20,160
120×120 pixels	24,801	40,460
80×80 pixels	59,151	87,500
Total	97,076	148,120

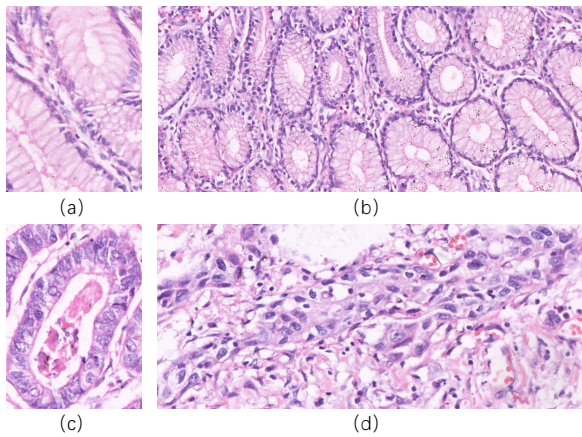


Figure 2: Example of Pathological images: (a)(b) Normal pathological images, (c) Non-invasive abnormal pathological image, (d) Invasive abnormal pathological image.

2.3. Database description

2.3.1. Normal image

Every normal image does not contain any cancerous area. In each normal image, each cell has no or very small atypia (Figure. 2 (a)). Moreover, the nuclei of the cells in the image have almost no mitosis and are regularly arranged in one layer (Figure. 2 (b)). Therefore, when observed under the optic microscope, if no cancellation of any cells and tissues is observed, and the characteristics of the normal image are satisfied, it can be judged that this is a normal image [16]. In the process of making normal image data set, because of the characteristics of normal images, we directly crop the whole image. The resulting images are shown in (a) (b) (c) in Figure. 3.

2.3.2. Abnormal image

Each abnormal image is a pathological image that consists of gastric cancer. Cancer in the stomach is irregular nodular and infiltrates into the surrounding tissues in the form of roots or crabs. It has a hard texture, and the section is often gray-white. When observed under a microscope, the cancer cells can be arranged in a nest, acinar, tubular, or cord shape, and the boundary with the stroma is generally clear (Figure. 2 (c)). However, when the cancer cells infiltrate into the stroma, the boundary between them is not clear (Figure. 2 (d)). Based on the above facts, when the cells are observed to form gland or adenoid structure with uneven size, different shape, and irregular arrangement, it can be judged that the pathological image is abnormal. In the abnormal images, the cells in the cancer area are often irregularly arranged in many layers, and the nuclei have different sizes and division phenomena [1, 17, 18]. In the process of making the abnormal image dataset, we crop every cancerous region selected according to the original ground truth (GT) images. Then all the cropped images are filtered according to whether there is more than 50% of the cancerous area in the images. The resulting images are shown in (d) (e) (f) in Figure. 3.

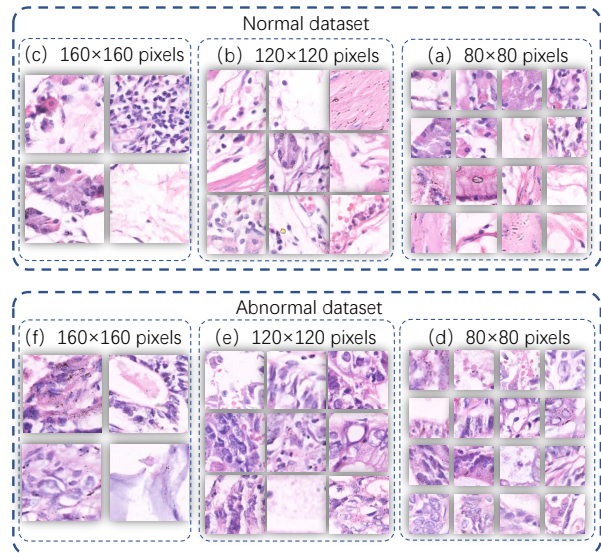


Figure 3: Example of GasHisSDB.

3. Evaluation of GasHisSDB

3.1. Methods of feature extraction

Extracting the various virtual features of a database is a pre-preparation for classification using a machine learning classifier. In this paper, we use five methods to extract the visual features of the database, including color histogram, luminance histogram, histogram of oriented gradient (HOG), local binary pattern (LBP), and gray level co-occurrence matrix (GLCM) features.

3.1.1. Color histogram and luminance histogram

Color histogram is the most commonly used method to describe color characteristics of images. It can simply represent the global distribution of colors in an image, i.e. the proportion of different colors in the whole image. It is especially suitable for describing images that are difficult to automatically segment and images that do not need to consider the spatial location of objects [19, 20]. Its advantage is that it is not affected by image rotation and shift changes, and further normalization is not affected by image scale changes. The disadvantage is that it cannot describe the local distribution of colors in the image and the spatial location of each color, that is, it cannot describe a specific object or object in the image. Luminance is a special color feature, and it is the average of three color components [21]. We take the histogram of luminance as luminance feature.

3.1.2. Texture features

The texture is a visual feature that reflects homogeneity in an image. It reflects the organization and arrangement of surface structures with slow or periodic changes on the surface of an object. It is not based on the characteristics of pixels but needs to carry out the statistical calculation on the region containing multiple pixels [22]. The texture is repre-

sented by the gray distribution of pixels and their surrounding spatial neighbor, that is, local texture information. Besides, global texture information is the degree of repetition of local texture information. This paper use three methods to describe texture features of GasHisSDB, which are HOG, LBP and GLCM.

HOG is a feature descriptor used for object detection in computer vision and image processing. It constructs features by calculating and statistics the gradient direction histogram of the local area of the image, detects feature descriptions of objects, and constructs features by calculating the gradient direction histogram of the local area of the image [23]. It has the advantage of maintaining splendid invariance in both geometric and optical distortion of the image because HOG operates on the local cells of an image. The whole image is divided into cells of the same size and not overlapping each other, and the gradient and direction of each cell are calculated. Then, the gradient direction of each pixel is divided into 9 bins on average from 0 to 180 degrees. By counting the gradient histogram of each cell, the descriptor of each cell is formed.

LBP is an effective texture description operator that measures and extracts textural information local to an image with significant advantages such as grey level invariance and rotational invariance, and the feature is easy to compute. The value of LBP for each pixel is eight values within its eight-neighbor compared to his pixel. If the pixel value in the eight-neighbor is greater than or equal to the central pixel value, the position is labeled by 1, and 0 for otherwise, aligning them clockwise after eight comparisons yield a binary number of eight lengths, yielding LBP values [24].

The Co-occurrence Matrix is defined by the joint probability density of the pixels at two locations. It not only reflects the distribution of brightness but also reflects the distribution of location between pixels with the same or near brightness. It is a second-order statistical feature about the change of image brightness. GLCM is the basis for defining a set of texture features [25, 26]. To more intuitively describe the texture state with a symbiotic matrix, some parameters reflecting the state of the matrix are derived from the symbiotic matrix, typically the following:

1. Contrast: Reflects the sharpness of the image and the depth of texture grooves.
2. Correlation: It measures the degree of similarity of spatial grayscale symbiosis matrix elements in a row or column directions.
3. Energy: It is the sum of squares of gray symbiosis matrix elements, so it is also called energy, which reflects the uniformity of gray distribution and texture thickness of the image.
4. Homogeneity: Returns a measure of the compactness of the diagonal distribution of elements in GLCM.

3.2. Classification

After the steps of feature extraction, seven classical machine learning methods are used to classify GasHisSDB, including Linear Regression, k -Nearest Neighbor (k NN), naive

Bayesian classifier, Random Forest (RF), linear Support Vector Machine (linear SVM), non-linear Support Vector Machine (non-linear SVM), and artificial neural network (ANN). Furthermore, four classical or novel deep learning methods are used to classify GasHisSDB, including VGG16, Inception-V3, ResNet50 and ViT.

3.2.1. Classical machine learning methods

The machine learning method for classification is to judge whether the image is normal or not by visual features. Linear Regression is a method to get a linear model as much as possible to accurately predict the real value output label. In Linear regression least square function is used to establish the relationship between one or more independent variables [27]. k NN is a simple and commonly used supervised learning method based on the distance to find the closest k samples to vote for the prediction result [28]. The naive Bayes classifier is a classifier based on the Bayesian decision theory in probability theory and adopts the attribute conditional independence assumption [29, 30]. RF is a parallel ensemble learning method and an extended variant of Bagging. RF is based on a decision tree learner, which adds random attribute selection to the training process of the decision tree [31]. SVMs are classified into linear and non-linear according to the kernel functions. Linear SVM maps training examples to points in space to maximize the gap between the two categories. Then, the new examples are mapped to the same space and predicted to belong to a category based on which side of the gap they fall on. In addition to performing linear classification, SVM can also use a kernel function to effectively perform non-linear classification, thereby implicitly mapping its input to a high-dimensional feature space [32, 33]. An ANN is a classification algorithm that is composed of a structure that simulates human brain neurons and is trained through a propagation algorithm [34].

3.2.2. Deep learning methods

The concept of deep learning originates from the research of ANNs, where a multi-layer perceptron with multiple hidden layers is a deep learning structure. Deep learning forms a more abstract high-level representation attribute category or feature by combining low-level features to discover distributed feature representations of data.

In 2014, the Visual Geometry Group and Google DeepMind developed a new deep convolutional neural network: VGG [35]. VGG is a *Convolutional Neural Network* (CNN) improved by AlexNet. Several forms of VGG models are released, and the most commonly used in the field of image classification is VGG16 one. In VGG16, three 3×3 convolution kernels are used instead of 7×7 convolution kernels, and two 3×3 convolution kernels are used instead of 5×5 convolution kernels. The main purpose of this structure is to ensure the same perceptual field conditions, enhance the depth of the network, and to a certain extent enhance the effect of the neural network.

Google's InceptionNet debuted in the 2014 ILSVRC competition. InceptionNet has developed multiple versions, of

Table 2

Classification results of five image features using different classifiers in the 160×160 pixels sub-database of GasHisSDB (In [%]). The bold text in the table indicates the highest value of the classification result of different classifiers for the same feature.

Features	Methods	Acc	Abnormal				Normal			
			Precision	Recall	Specificity	F1-score	Precision	Recall	Specificity	F1-score
Color histogram	LR	83.29	81.32	80.42	85.54	80.87	84.80	85.54	80.42	85.17
	kNN	85.52	82.95	84.35	86.43	83.64	87.58	86.43	84.35	87.01
	RF	85.99	81.65	87.83	84.55	84.63	89.88	84.55	87.83	87.13
	linear SVM	41.12	33.92	35.96	45.16	34.91	47.40	45.16	35.96	46.25
	non-linear SVM	56.09	Null	0.00	100.00	0.00	56.09	100.00	0.00	71.87
	ANN	78.89	77.78	72.68	83.75	75.14	79.67	83.75	72.68	81.66
lumiNullce histogram	LR	70.97	67.95	49.92	84.67	57.56	72.21	84.67	49.92	77.95
	kNN	77.10	70.30	72.60	80.03	71.43	81.78	80.03	72.60	80.90
	RF	79.13	72.17	76.60	80.78	74.32	84.14	80.78	76.60	82.42
	linear SVM	42.34	40.50	98.67	5.68	57.43	86.74	5.68	98.67	10.66
	non-linear SVM	60.58	Null	0.00	100.00	0.00	60.58	100.00	0.00	75.45
	ANN	71.23	64.74	59.34	78.97	61.92	74.90	78.97	59.34	76.88
HOG	LR	60.46	48.96	7.20	95.11	12.56	61.16	95.11	7.20	74.45
	kNN	61.42	51.31	41.65	74.28	45.98	66.17	74.28	41.65	69.99
	naive Bayesian	54.43	45.11	71.84	43.11	55.42	70.17	43.11	71.84	53.40
	RF	60.85	50.33	53.01	65.95	51.63	68.32	65.95	53.01	67.11
	linear SVM	53.28	44.82	80.14	35.79	57.49	73.47	35.79	80.14	48.13
	non-linear SVM	60.58	Null	0.00	100.00	0.00	60.58	100.00	0.00	75.45
LBP	ANN	61.54	54.30	15.40	91.57	23.99	62.45	91.57	15.40	74.26
	LR	74.29	69.32	62.42	82.02	65.69	77.03	82.02	62.42	79.45
	kNN	70.21	66.11	50.11	83.28	57.01	71.95	83.28	50.11	77.20
	naive Bayesian	57.71	47.78	78.28	44.32	59.34	75.82	44.32	78.28	55.94
	RF	70.27	62.16	62.84	75.10	62.50	75.64	75.10	62.84	75.37
	linear SVM	48.17	36.83	44.02	50.87	40.10	58.27	50.87	44.02	54.32
GLCM	non-linear SVM	60.58	Null	0.00	100.00	0.00	60.58	100.00	0.00	75.45
	ANN	71.84	67.38	55.41	82.54	60.81	73.99	82.54	55.41	78.03
	LR	67.73	59.71	55.75	75.52	57.67	72.40	75.52	55.75	73.93
	kNN	69.26	62.30	55.79	78.03	58.87	73.06	78.03	55.79	75.46
	naive Bayesian	61.99	51.12	82.01	48.96	62.98	80.70	48.96	82.01	60.94
	RF	71.39	63.16	65.85	75.00	64.48	77.14	75.00	65.85	76.06
GLCM	linear SVM	66.50	55.89	71.27	63.39	62.65	77.22	63.39	71.27	69.63
	non-linear SVM	67.76	58.77	61.05	72.12	59.89	73.99	72.12	61.05	73.05
	ANN	68.69	60.64	58.65	75.22	59.63	73.65	75.22	58.65	74.43

which Inception-V3 is a more representative version in this large family [36]. The main idea of the Inception architecture is to find out how to use dense components to approximate the optimal local sparse nodes. Inception-V2 also draws on the design ideas of VGGNet, replacing the 5×5 large convolution with two 3×3 convolutions. Besides, the famous BatchNormalization is also proposed for the first time. Secondly, Inception-V3 also introduces the method of splitting a larger two-dimensional convolution into two smaller one-dimensional convolutions.

In 2016, to solve the difficulty of training deep networks due to the disappearance of gradients, Kaiming He et al. proposed various forms of ResNet [37]. The most commonly used in the field of image classification is ResNet50. The ResNet50 team separately constructed a ResNet50 building block with "Shortcut Connection" and a down-sampling ResNet50 building block. A 1×1 convolution operation is added to the main branch of the regional down-sampling building block.

In 2020, Alexey Dosovitskiy et al. proposed the ViT model [38]. By using the Transformer, which is very effective in the field of natural language processing, it is demon-

strated that the image classification domain can reduce the dependence on CNNs. ViT crops an image into small chunks and provides a sequence of linear embeddings of these chunks as input to the Transformer and trains the model in a supervised manner for image classification.

3.3. Evaluation of classical machine learning methods

In this paper, various classification experiments are conducted on 160×160 pixels, 120×120 pixels and 80×80 pixels GasHisSDB database to verify the performance of different classifiers on GasHisSDB. In this part, Table. 2, Table. 3 and Table. 4 show the comparison results of all the above-mentioned classical machine learning methods. All the different feature classification comparison experiments use the same parameters. In kNN, k is set to 9. The number of trees in the RF is set to 10. The kernel function of the non-linear SVM is a Gaussian kernel. ANN uses a 2-layer network, the number of nodes in the first layer is 10 and in the second layer is 3. The number of epochs of ANN training is set to 500, the learning rate is set to 0.01 and the expected loss is

Table 3

Classification results of five image features using different classifiers in the 120×120 pixels sub-database of GasHisSDB (In [%]). The bold text in the table indicates the highest value of the classification result of different classifiers for the same feature.

Features	Methods	Acc	Abnormal				Normal			
			Precision	Recall	Specificity	F1-score	Precision	Recall	Specificity	F1-score
Color histogram	LR	83.46	80.01	75.28	88.47	77.57	85.38	88.47	75.28	86.90
	kNN	86.32	82.28	81.55	89.24	81.92	88.75	89.24	81.55	88.99
	RF	86.08	80.36	83.87	87.43	82.08	89.84	87.43	83.87	88.62
	linear SVM	46.28	39.48	77.62	27.06	52.34	66.36	27.06	77.62	38.45
	non-linear SVM	62.00	Null	0.00	100.00	0.00	62.00	100.00	0.00	76.54
	ANN	81.20	78.14	70.14	87.98	73.93	82.78	87.98	70.14	85.30
lumiNullce histogram	LR	71.28	66.89	48.39	85.32	56.15	72.95	85.32	48.39	78.65
	kNN	76.43	68.19	71.17	79.65	69.65	81.84	79.65	71.17	80.73
	RF	77.60	69.36	73.57	80.08	71.40	83.17	80.08	73.57	81.60
	linear SVM	58.54	47.45	84.62	42.55	60.80	81.86	42.55	84.62	55.99
	non-linear SVM	62.00	Null	0.00	100.00	0.00	62.00	100.00	0.00	76.54
	ANN	71.18	62.97	58.65	78.86	60.73	75.68	78.86	58.65	77.23
HOG	LR	61.78	33.72	0.58	99.30	1.15	61.97	99.30	0.58	76.31
	kNN	62.02	50.04	39.56	75.79	44.18	67.17	75.79	39.56	71.22
	naive Bayesian	54.83	44.29	73.06	43.66	55.15	72.56	43.66	73.06	54.52
	RF	60.55	48.15	49.62	67.25	48.87	68.53	67.25	49.62	67.88
	linear SVM	50.91	39.90	57.60	46.81	47.14	64.30	46.81	57.60	54.18
	non-linear SVM	62.00	Null	0.00	100.00	0.00	62.00	100.00	0.00	76.54
LBP	ANN	62.35	54.37	5.77	97.03	10.43	62.69	97.03	5.77	76.17
	LR	73.34	67.20	58.29	82.56	62.43	76.35	82.56	58.29	79.34
	kNN	70.27	64.05	49.64	82.92	55.93	72.87	82.92	49.64	77.57
	naive Bayesian	57.39	46.41	78.43	44.49	58.31	77.09	44.49	78.43	56.42
	RF	70.13	60.88	59.90	76.41	60.39	75.66	76.41	59.90	76.03
	linear SVM	46.21	29.70	30.40	55.89	30.05	56.71	55.89	30.40	56.30
GLCM	non-linear SVM	62.00	Null	0.00	100.00	0.00	62.00	100.00	0.00	76.54
	ANN	71.19	64.72	53.19	82.23	58.39	74.13	82.23	53.19	77.97
	LR	67.54	58.21	51.65	77.27	54.74	72.28	77.27	51.65	74.69
	kNN	69.79	61.98	53.04	80.05	57.16	73.56	80.05	53.04	76.67
	naive Bayesian	61.40	49.52	80.77	49.53	61.39	80.77	49.53	80.77	61.41
	RF	71.15	61.42	64.72	75.09	63.03	77.64	75.09	64.72	76.34
GLCM	linear SVM	66.66	55.02	67.30	66.28	60.54	76.78	66.28	67.30	71.14
	non-linear SVM	69.43	60.08	58.27	76.27	59.16	74.88	76.27	58.27	75.57
	ANN	68.10	58.45	55.56	75.79	56.97	73.56	75.79	55.56	74.66

set to 0.01.

3.3.1. On 160 × 160 pixels sub-database

This section focuses on the classification results of classical machine learning methods for the 160×160 sub-database. According to Table. 2, the color histogram is the extracted feature with the most feature items.

The color histogram obtains the best classification accuracy in the classification results of different classifiers using five different features on all 160×160 sub-database in the RF, which is 85.99%. In addition, in the color histogram, the classification accuracy of the three classifiers reached around 80%, which are LR, kNN and ANN. All SVM classifiers perform poorly on the color histogram features. However, the color histogram on GasHisSDB, the naive Bayesian classifier cannot get the classification effect because of the existence of a large number of low luminance statistics with zero values in the three color channels.

The luminance as the mean value of the color and its histogram as a feature does not gain a better classification accuracy. Because of this, the luminance histogram also has the

above problem on the naive Bayesian classifier. The classification results of the naive Bayesian classifier for these two color features are therefore not presented in the table. RF shows robustness in two features, and also obtains the highest accuracy rate of 79.13% in using the luminance histogram for classification. However, the LR, kNN and ANN classifiers that perform better on the color histogram have a significant drop in accuracy on the luminance histogram.

The classification effect of HOG on all classifiers is not very effective and the accuracy rate is very dense, the difference is not much distributed between 53%-62%.

On the contrary, the distribution of LBP image classification accuracy is particularly scattered, with the highest Linear Regression classifier reaching 74.29%, followed by ANN reaching 71.84%. The lowest linear SVM classification effect is less than 50%.

The classification effect of the four statistic values of GLCM is 71.39% only for RF, and other classifiers are also above 60%. It is worth noting that the accuracy of non-linear SVM with other features except color histogram and GLCM has not changed at all, which is 60.58%. The accuracy of

Table 4

Classification results of five image features using different classifiers in the 80×80 pixels sub-database of GasHisSDB (In [%]). The bold text in the table indicates the highest value of the classification result of different classifiers for the same feature.

Features	Methods	Acc	Abnormal				Normal			
			Precision	Recall	Specificity	F1-score	Precision	Recall	Specificity	F1-score
Color histogram	LR	82.22	78.17	77.59	85.35	77.88	84.93	85.35	77.59	85.14
	kNN	85.24	80.60	83.52	86.41	82.03	88.58	86.41	83.52	87.48
	RF	83.27	77.14	83.15	83.34	80.03	87.98	83.34	83.15	85.60
	linear SVM	60.81	50.86	83.58	45.41	63.24	80.36	45.41	83.58	58.03
	non-linear SVM	59.67	Null	0.00	100.00	0.00	59.67	100.00	0.00	74.74
	ANN	79.28	76.60	70.03	85.54	73.17	80.85	85.54	70.03	83.13
lumiNullce histogram	LR	70.16	66.79	51.77	82.60	58.33	71.70	82.60	51.77	76.76
	kNN	74.65	67.67	71.11	77.04	69.35	79.78	77.04	71.11	78.38
	RF	75.10	67.77	72.94	76.55	70.26	80.71	76.55	72.94	78.58
	linear SVM	54.58	46.58	85.81	33.47	60.38	77.72	33.47	85.81	46.79
	non-linear SVM	59.67	Null	0.00	100.00	0.00	59.67	100.00	0.00	74.74
	ANN	70.17	63.19	62.38	75.43	62.78	74.79	75.43	62.38	75.11
HOG	LR	59.87	53.42	3.96	97.67	7.37	60.07	97.67	3.96	74.39
	kNN	59.63	49.95	42.22	71.40	45.76	64.64	71.40	42.22	67.85
	naive Bayesian	55.91	46.97	72.35	44.79	56.96	70.56	44.79	72.35	54.79
	RF	59.08	49.31	51.88	63.95	50.56	66.28	63.95	51.88	65.10
	linear SVM	53.47	44.46	61.60	47.98	51.64	64.89	47.98	61.60	55.17
	non-linear SVM	59.70	90.91	0.08	99.99	0.17	59.68	99.99	0.08	74.75
	ANN	59.67	50.08	2.49	98.32	4.75	59.87	98.32	2.49	74.42
LBP	LR	70.92	65.32	59.49	78.65	62.27	74.17	78.65	59.49	76.34
	kNN	68.48	63.20	52.32	79.41	57.24	71.13	79.41	52.32	75.04
	naive Bayesian	59.09	49.55	77.69	46.52	60.51	75.52	46.52	77.69	57.57
	RF	68.16	60.13	62.49	71.98	61.29	73.95	71.98	62.49	72.95
	linear SVM	43.10	27.68	25.48	55.01	26.53	52.20	55.01	25.48	53.56
	non-linear SVM	59.67	Null	0.00	100.00	0.00	59.67	100.00	0.00	74.74
	ANN	68.57	62.75	54.32	78.21	58.23	71.69	78.21	54.32	74.81
GLCM	LR	65.56	57.32	57.24	71.19	57.28	74.65	71.21	64.23	72.89
	kNN	68.84	62.32	57.53	76.49	59.83	72.71	76.49	57.53	74.55
	naive Bayesian	62.12	51.96	80.87	49.45	63.27	79.27	49.45	80.87	60.91
	RF	68.39	60.13	64.23	71.21	62.11	74.65	71.21	64.23	72.89
	linear SVM	66.82	57.14	71.04	63.97	63.33	76.57	63.97	71.04	69.71
	non-linear SVM	68.31	61.03	59.26	74.42	60.13	72.99	74.42	59.26	73.70
	ANN	65.52	56.70	61.40	68.30	58.96	72.36	68.30	61.40	70.27

the color histogram's non-linear SVM classifier is 56.09% and the accuracy of GLCM's non-linear SVM classifier is 67.76%.

3.3.2. On 120 × 120 pixels sub-database

In this chapter, we focus on the comparison of the experimental results of the 120 × 120 pixels sub-database. The experimental results are shown in Table. 3. In general, compared with 160 × 160 pixels sub-database classification results, 120 × 120 pixels sub-database classification results except for the color histogram, the rest of the best classifiers remain unchanged.

The four better-performing classifiers on the color histogram feature still perform better, and the accuracy rate fluctuates slightly, resulting in the kNN classifier reaching the best accuracy rate of 86.32%. The classification performance of the two SVM classifiers on the features of the color histogram is still not ideal. Naive Bayesian classifier is still not suitable for color histogram and luminance histogram features. The linear SVM effect of the luminance histogram classifier has been greatly improved in the classification of the 120 × 120 pixels sub-database. The accuracy of other

classifiers on the features of the luminance histogram has little change. The HOG feature still does not perform well in every classifier. The highest accuracy rate is only 62.35% of ANN. The classification results of LBP and GLCM features are similar to the classification effect on the 160 × 160 pixels sub-database. The best accuracy rate on LBP is a linear regression with a precision rate of 73.34%. The best accuracy rate on GLCM is that the RF reaches 71.15%. Similarly, the non-linear SVM of 120 × 120 pixels sub-database also has the problem of constant accuracy of multiple features.

3.3.3. On 80 × 80 pixels sub-database

The classification results of the 80 × 80 pixels sub-database are shown in Table. 4. The overall best classifier on each feature remains the same as that of the best classifier for each feature corresponding to the 120 × 120 pixels sub-database except for HOG features that have a small gap between each classifier.

Compared with the classification results of the other two sub-databases, the classification effect of each classifier on the color histogram and the luminance histogram has no particularly large fluctuations. It confirms the consistency of the

Table 5

Classification results of four deep learning classifiers on GasHisSDB (In [%]). The bold text in the table indicates the maximum value or the best index of the classification results of different categories.

Sub-database Size	Model	Quantity of epoch	Model size(MB)	best epoch	training time(s)	Acc	Category	Precision	Recall	Specificity	F1-score	
160 × 160 pixels	VGG16	100	268.16	100	13873	95.90	Abnormal	93.8	96.0	95.9	94.9	
							Normal	97.3	95.9	96.0	96.6	
	Inception-V3	100	89.69	92	10296	94.57	Abnormal	94.1	92.0	96.2	93.0	
							Normal	94.9	96.2	92.0	95.5	
	ResNet50	100	83.12	84	10023	96.09	Abnormal	94.6	95.6	96.4	95.1	
							Normal	97.1	96.4	95.6	96.7	
		ViT	100	31.17	97	2587	86.21	Abnormal	83.8	80.6	89.9	82.2
			Normal	87.7	89.9	80.6	88.8					
	ViT	400	31.17	399	10014	92.23	Abnormal	92.1	87.8	95.1	89.9	
		Normal	92.3	95.1	87.8	93.7						
	120 × 120 pixels	VGG16	100	268.16	100	26105	96.47	Abnormal	96.7	94.0	98.0	95.3
								Normal	96.4	98.0	94.0	97.2
Inception-V3		100	89.69	98	19719	95.83	Abnormal	94.6	94.4	96.7	94.5	
							Normal	96.6	96.7	94.4	96.6	
ResNet50		100	83.12	94	19087	95.94	Abnormal	96.2	93.0	97.8	94.6	
							Normal	95.8	97.8	93.0	96.8	
		ViT	100	31.17	100	4077	89.44	Abnormal	87.0	84.9	92.2	85.9
			Normal	90.9	92.2	84.9	91.5					
ViT		500	31.17	496	20410	94.59	Abnormal	93.5	93.4	95.3	93.2	
		Normal	95.4	95.9	92.5	95.6						
80 × 80 pixels		VGG16	100	268.16	90	62152	96.12	Abnormal	94.2	96.3	96.0	95.2
								Normal	97.4	96.0	96.3	96.7
	Inception-V3	100	89.69	99	43926	95.41	Abnormal	95.5	93.0	97.0	94.2	
							Normal	95.3	97.0	93.0	96.1	
	ResNet50	100	83.12	97	41992	96.09	Abnormal	96.2	94.0	97.5	95.1	
							Normal	96.0	97.5	94.0	96.7	
		ViT	100	31.17	89	8247	90.23	Abnormal	86.3	90.1	90.3	88.2
			Normal	93.1	90.3	90.1	91.7					
	ViT	500	31.17	496	41135	94.57	Abnormal	93.1	93.4	95.3	93.2	
		Normal	95.6	95.3	93.4	95.4						

three databases of GasHisSDB.

The classification accuracy of the color histogram is still polarized. The four excellent classifiers reach about 80%, and the other two are about 60%. RF still shows robustness in the task of luminance histogram classification and is the best classifier with an accuracy of 75.10%. The classification accuracy distribution of HOG features is denser than that of the other two sub-databases. The highest is only 59.87%. Due to the reduced sample size, each classifier has different degrees of accuracy reduction in addition to the naive Bayesian classifier for LBP features and GLCM features. The best classifier for LBP feature is still linear regression which reaches 70.92%. The highest accuracy rate of LBP feature has become 68.84% of k NN. In the classification results of the 80 × 80 pixels sub-database, the Bayesian algorithm of the color histogram and the luminance histogram is not applicable, and the problem that the nonlinear classifier is invariant to the non-GLCM algorithm still exists.

3.4. Evaluation of deep learning methods

In this part, classical and novel deep learning methods are used to classify the 160 × 160 pixels sub-database, 120 ×

120 pixels sub-database and 80 × 80 pixels sub-database of GasHisSDB. In a series of comparative experiments, the ratio of the training, validation and test sets to the three sub-databases is split 4:4:2. Each model uses a learning rate of 0.00002, the batch size is set to 32, and the experiment is performed for 100 epochs, to observe the classification results of this database on different models. The results of the comparative experiment are shown in Table. 5.

3.4.1. On 160 × 160 pixels sub-database

In general, deep learning models are far superior to classical machine learning methods, and even the lowest ViT accuracy is still higher than the highest accuracy of classical machine learning methods. The accuracy of the VGG model is more than 95%, but it has the longest training time and the model size is much larger than other deep learning models. The accuracy of Inception-V3 is slightly lower than that of VGG16. The accuracy of ResNet50 is slightly higher than that of VGG16, which is the highest value among all methods reaching 96.09%. Both the model size and training time of Inception-V3 and ResNet50 are better than VGG16 and the gap between the two is very close. ViT is the latest

model based on transformer structure. Its accuracy is at least 86.21%, but it is still higher than the classification accuracy of k NN on the color histogram. Importantly, compared to ResNet, ViT achieves such accuracy in only 1/4 of the training time and 1/3 of the model size. Moreover, the accuracy curve still has an increasing trend and the loss function still has not fully converged.

3.4.2. On 120×120 pixels sub-database

Because there are more training samples, VGG16 is the classifier with the highest accuracy in the classification results of the deep learning method of 120×120 pixels sub-database, which is 96.47%. The corresponding training time has also become twice that of 160×160 pixels sub-database. Inception-V3 and ResNet50 almost caught up with the accuracy rate of VGG16. The accuracy rates of Inception-V3 and ResNet50 are 95.83% and 95.94%, respectively. ViT also obtains a certain accuracy improvement when the amount of training data increased, reaching 89.44%.

3.4.3. On 80×80 pixels sub-database

The 80×80 pixels sub-database is the sub-database with the largest number of samples. The accuracy of the four classifiers has only slightly changed. The classification model with the highest accuracy rate is still 96.12% for VGG16. The lowest accuracy rate is still the ViT model with the least training time, which is 90.23%. However, the training time of ViT in the 80 sub-database has almost become 13.26% of the training time of VGG16 with the highest accuracy.

3.5. Additional experiment

Since it is observed that ViT did not fully converge in 100 epochs, a series of additional experiments are performed in this section. The experimental results are shown in the last item of each sub-database in Table. 5. In the follow-up additional experiment of 160×160 pixels sub-database, under the same parameter conditions, the training time is controlled to be similar to that of Inception-V3 and ResNet with running 100 epochs, so ViT needed to run 400 epochs. This experiment achieved an accuracy of 92.23%. Moreover, as the amount of data increases, when the control training time is the same as Inception-V3 and ResNet50, the accuracy of the ViT model with 120×120 pixels sub-database and 80×80 pixels sub-database is increased to 94.59% and 94.57%. These image classification results have reached the general level of medical image classification, and the ViT model is excellent in terms of model size.

3.6. discussion

In this chapter, we focus on the comparison of the classification results of the classifier from Linear Regression to Visual Transformer on the 160×160 pixels sub-database, 120×120 pixels sub-database and 80×80 pixels sub-database of GasHisSDB. Each method has a completely different classification performance on GasHisSDB. Classical machine learning methods have strict theoretical foundations, simple ideas, and excellent performance in some specific features and algorithms. However, deep learning methods are still far

ahead of classic machine learning methods in terms of image classification accuracy and experimental workload. As a subsize image database, GasHisSDB can be proved to have very complex performance in a variety of methods.

4. Conclusion and futures works

In this paper, a subsize image database of gastric histopathological images is developed, namely GasHisSDB. GasHisSDB has three sub-databases, 160×160 pixels sub-database, 120×120 pixels sub-database and 80×80 pixels sub-database. Each sub-database contains two folders of normal images and abnormal images. Each folder contains cropped images that have been renamed and shuffled. GasHisSDB has the function of testing the results of image classification. This paper is divided into the following two parts for testing. For classical machine learning methods, this paper extracts five different features. Then test the classification performance of seven different classification methods on three sub-databases, and analyze the differences in the accuracy of each classifier. For deep learning methods, this paper tests three repeatedly proven CNN methods and ViT, which has only recently been used in the field of image classification. This paper focuses on the analysis of the four models from the accuracy rate, model size, training time and other indicators. In addition, this paper conducts additional experiments for training time to find the best classification performance of ViT on GasHisSDB. The performance demonstrated by GasHisSDB in the image classification experiments in this paper is competent for the task of testing existing image classification methods.

The creation of the dataset means that more image classification methods can be used for this dataset. We will try newer image classification methods on GasHisSDB, and perform comparison and analysis of image classification methods to obtain better practical methods to contribute to the medical progress.

5. Acknowledgements

This work is supported by the "National Natural Science Foundation of China" (No. 61806047) and the "Fundamental Research Funds for the Central Universities" (No. N2019003). We also thank Miss. Zixian Li and Mr. Guoxian Li for their important discussion in this work.

References

- [1] Feng Hua Wang, L. Shen, J. Li, Zhi Wei Zhou, H. Liang, Xiao Tian Zhang, L. Tang, Y. Xin, J. Jin, and Yu Jing Zhang. The chinese society of clinical oncology (csc): Clinical guidelines for the diagnosis and treatment of gastric cancer. *Cancer Communications*, 39(1), 2019.
- [2] Hyuna Sung, Jacques Ferlay, Rebecca L. Siegel, Mathieu Laversanne, Isabelle Soerjomataram, Ahmedin Jemal, and Freddie Bray. Global cancer statistics 2020: GLOBOCAN estimates of incidence and mortality worldwide for 36 cancers in 185 countries. *CA: A Cancer Journal for Clinicians*, 0(0):1–41, 2021.
- [3] Tom, Waddell, Marcel, Verheij, William, Allum, David, Cunningham, Andrés, and Cervantes. Gastric cancer†: Esmo–esso–estro clin-

- ical practice guidelines for diagnosis, treatment and follow-up. *Radiotherapy and Oncology*, 2014.
- [4] Jack Rose Rolf Zeller Andrew H Fischer, Kenneth A Jacobson. Hematoxylin and eosin staining of tissue and cell sections. *CSH protocols*, 2008.
- [5] John K C Chan. The wonderful colors of the hematoxylin-eosin stain in diagnostic surgical pathology. *Int J Surg Pathol*, 22(1):12–32, 2014.
- [6] Robert D Cardiff, Claramae H Miller, and Robert J Munn. Manual hematoxylin and eosin staining of mouse tissue sections. *Cold Spring Harbor protocols*, 2014(6):655–658, 2014.
- [7] Vinay Kumar, Abul K Abbas, and Jon C Aster. *Robbins basic pathology e-book*. Elsevier Health Sciences, 2017.
- [8] David Forsyth and Jean Ponce. Computer vision: A modern approach., 2011.
- [9] Andrianos Tsekrekos, Sönke Detlefsen, Robert Riddell, James Conner, Luca Mastracci, Kieran Sheahan, Jayant Shetye, Lars Lundell, and Michael Vieth. Histopathologic tumor regression grading in patients with gastric carcinoma submitted to neoadjuvant treatment: results of a delphi survey. *Human pathology*, 84:26–34, 2019.
- [10] Peng Jin, Xiaoyan Ji, Wenzhe Kang, Yang Li, Hao Liu, Fuhai Ma, Shuai Ma, Haitao Hu, Weikun Li, and Yantao Tian. Artificial intelligence in gastric cancer: A systematic review. *Journal of Cancer Research and Clinical Oncology*, pages 1–12, 2020.
- [11] E. Miranda, M. Aryuni, and E. Irwansyah. A survey of medical image classification techniques. In *2016 International Conference on Information Management and Technology (ICIMTech)*, pages 56–61, 2016.
- [12] Carlos Affonso, André Luis Debiasso Rossi, Fábio Henrique Antunes Vieira, André Carlos Ponce de Leon Ferreira, et al. Deep learning for biological image classification. *Expert Systems with Applications*, 85:114–122, 2017.
- [13] Hiral Kotadiya and Darshana Patel. Review of medical image classification techniques. In *Third International Congress on Information and Communication Technology*, pages 361–369. Springer, 2019.
- [14] Yuexiang Li, Xuechen Li, Xinpeng Xie, and Linlin Shen. Deep learning based gastric cancer identification. In *2018 IEEE 15th International Symposium on Biomedical Imaging (ISBI 2018)*, pages 182–185. IEEE, 2018.
- [15] Changhao Sun, Chen Li, Jinghua Zhang, Md Mamunur Rahaman, Shiliang Ai, Hao Chen, Frank Kulwa, Yixin Li, Xiaoyan Li, and Tao Jiang. Gastric histopathology image segmentation using a hierarchical conditional random field. *Biocybernetics and Biomedical Engineering*, 40(4):1535–1555, 2020.
- [16] Sharon W Weiss, John R Goldblum, and Andrew L Folpe. *Enzinger and Weiss's soft tissue tumors*. Elsevier Health Sciences, 2007.
- [17] Japanese Gastric Cancer Association jgca@ koto. kpu-m. ac. jp. Japanese classification of gastric carcinoma: 3rd english edition. *Gastric cancer*, 14:101–112, 2011.
- [18] Tsunehiro Takahashi, Yoshiro Saikawa, and Yuko Kitagawa. Gastric cancer: current status of diagnosis and treatment. *Cancers*, 5(1):48–63, 2013.
- [19] Theo Gevers, Joost Van De Weijer, and Harro Stokman. Color feature detection, 2006.
- [20] Joost Van De Weijer and Cordelia Schmid. Coloring local feature extraction. In *European conference on computer vision*, pages 334–348. Springer, 2006.
- [21] Ze Lu, Xudong Jiang, and Alex Kot. Color space construction by optimizing luminance and chrominance components for face recognition. *Pattern Recognition*, 83:456–468, 2018.
- [22] Mona Sharma and Sameer Singh. Evaluation of texture methods for image analysis. In *The Seventh Australian and New Zealand Intelligent Information Systems Conference, 2001*, pages 117–121. IEEE, 2001.
- [23] Yanwei Pang, Yuan Yuan, Xuelong Li, and Jing Pan. Efficient hog human detection. *Signal Processing*, 91(4):773–781, 2011.
- [24] Shu-Ren Zhou and Jian-Ping Yin. Lbp texture feature based on haar characteristics. *Journal of Software*, 24(8):1909–1926, 2013.
- [25] P Mohanaiah, P Sathyanarayana, and L GuruKumar. Image texture feature extraction using glm approach. *International journal of scientific and research publications*, 3(5):1–5, 2013.
- [26] HOU Qunqun, WANG Fei, and YAN Li. Extraction of color image texture feature based on gray-level co-occurrence matrix. *Remote Sensing for Land & Resources*, 25(4):26–32, 2013.
- [27] Douglas C Montgomery, Elizabeth A Peck, and G Geoffrey Vining. *Introduction to linear regression analysis*. John Wiley & Sons, 2021.
- [28] Leif E Peterson. K-nearest neighbor. *Scholarpedia*, 4(2):1883, 2009.
- [29] Irina Rish et al. An empirical study of the naive bayes classifier. In *IJCAI 2001 workshop on empirical methods in artificial intelligence*, volume 3, pages 41–46, 2001.
- [30] Daniel Berrar. Bayes' theorem and naive bayes classifier. *Encyclopedia of Bioinformatics and Computational Biology: ABC of Bioinformatics*; Elsevier Science Publisher: Amsterdam, The Netherlands, pages 403–412, 2018.
- [31] Andy Liaw, Matthew Wiener, et al. Classification and regression by randomforest. *R news*, 2(3):18–22, 2002.
- [32] William S Noble. What is a support vector machine? *Nature biotechnology*, 24(12):1565–1567, 2006.
- [33] Shan Suthaharan. Support vector machine. In *Machine learning models and algorithms for big data classification*, pages 207–235. Springer, 2016.
- [34] Mohamad H Hassoun et al. *Fundamentals of artificial neural networks*. MIT press, 1995.
- [35] Karen Simonyan and Andrew Zisserman. Very deep convolutional networks for large-scale image recognition. *arXiv preprint arXiv:1409.1556*, 2014.
- [36] Christian Szegedy, Vincent Vanhoucke, Sergey Ioffe, Jon Shlens, and Zbigniew Wojna. Rethinking the inception architecture for computer vision. In *Proceedings of the IEEE conference on computer vision and pattern recognition*, pages 2818–2826, 2016.
- [37] Kaiming He, Xiangyu Zhang, Shaoqing Ren, and Jian Sun. Deep residual learning for image recognition. In *Proceedings of the IEEE conference on computer vision and pattern recognition*, pages 770–778, 2016.
- [38] Alexey Dosovitskiy, Lucas Beyer, Alexander Kolesnikov, Dirk Weissenborn, Xiaohua Zhai, Thomas Unterthiner, Mostafa Dehghani, Matthias Minderer, Georg Heigold, Sylvain Gelly, et al. An image is worth 16x16 words: Transformers for image recognition at scale. *arXiv preprint arXiv:2010.11929*, 2020.